Fusion, collapse, and stationary bound states of incoherently coupled waves in bulk cubic media

O. Bang,[1] L. Bergé,[2] and J. Juul Rasmussen[3]
[1]*Australian Photonics Cooperative Research Centre, Research School of Physical Sciences and Engineering, Optical Sciences Centre, Australian National University, Canberra, Australian Capital Territory 0200, Australia*
[2]*Commissariat à l'Energie Atomique, CEA/Bruyères-le-Châtel, Boîte Postale 12, 91680 Bruyères-le-Châtel, France*
[3]*Risø National Laboratory, Optics and Fluid Dynamics Department, OFD-128 P.O. Box 49, DK-4000 Roskilde, Denmark*
(Received 16 October 1998)

We study the interaction between two localized waves that propagate in a bulk (two transverse dimensions) Kerr medium, while being incoherently coupled through cross-phase modulation. The different types of stationary solitary wave solutions are found and their stability is discussed. The results of numerical simulations suggest that the solitary waves are unstable. We derive sufficient conditions for when the wave function is bound to collapse or spread out, and we develop a theory to describe the regions of different dynamical behavior. For localized waves with the same center we confirm these sufficient conditions numerically and show that only when the equations and the initial conditions are symmetric are they also close to being necessary conditions. Using Gaussian initial conditions we predict and confirm numerically the power-dependent characteristic initial separations that divide the phase space into collapsing and diffracting solutions, and further divide each of these regions into subregions of coupled (fusion) and uncoupled dynamics. Finally we illustrate how, close to the threshold of collapse, the waves can cross several times before eventually collapsing or diffracting. [S1063-651X(99)00604-2]

PACS number(s): 42.65.Tg, 42.65.Sf, 42.65.Jx, 42.60.Jf

I. INTRODUCTION

When two or more localized light waves copropagate inside a centrosymmetric optical bulk medium, they can interact strongly through the cubic nonlinear Kerr effect. The nature of the interaction will depend on the state of the waves, i.e., their frequency and polarization, as well as on the structure of the third-order susceptibility tensor. If we neglect higher-order effects such as loss and four-wave mixing, we can write the dynamical equations in the general normalized form (see, e.g., [1])

$$i(\partial_z+\vec{v}_n\cdot\vec{\nabla})E_n+\sigma_n\nabla^2E_n+I_nE_n=0,$$
$$I_n=\sum_{j=1}^{N}\gamma_{jn}|E_j|^2. \tag{1}$$

Here $E_n(\vec{r},z)$ is the slowly varying envelope of the nth component, $n=[1,N]$, of the electric field, which is propagating along the z axis and diffracting in the two-dimensional (2D) transverse plane $\vec{r}=(x,y)$, with $\vec{\nabla}=(\partial_x,\partial_y)$ and $\nabla^2=\partial_x^2+\partial_y^2$. The real parameters σ_n determine the strength of the diffraction, whereas the real nonlinearity parameters γ_{jn} determine the strength of the self-phase modulation (SPM) for $j=n$ and the cross-phase modulation (XPM) for $j\neq n$. The effect of linear walk-off, characterized by the real vectors $\vec{v}_n=(v_{nx},v_{ny})$, can be removed by the simple unitary transformation

$$E_n\rightarrow E_n\exp[i(|\vec{v}_n|^2z-2\vec{v}_n\cdot\vec{r})/(4\sigma_n)].$$

However, for the sake of clarity we keep the walk-off terms in Eqs. (1) during the discussion of its different applications for describing the dynamics of 2D localized waves. Note that the walk-off could not be removed if the four-wave-mixing terms had been included in the model, i.e., if two or more components had been phase matched.

For a single component, $N=1$, Eqs. (1) reduce to the well-known cubic nonlinear Schrödinger (NLS) equation, which is the fundamental model for numerous physical situations, i.e., for all nearly monochromatic wave packets in strongly dispersive, weakly nonlinear media [2]. In 1D the NLS equation is integrable and has stable soliton solutions [3], whereas all localized solutions are inherently unstable in 2D and will either diffract or self-focus until a catastrophic collapse occurs at a finite propagation distance. A sufficient condition for collapse for $\sigma_1\gamma_{11}>0$, which is the case we are interested in here, is that the Hamiltonian for the system is negative. This leads to a necessary condition for collapse in terms of the power $P_1=\int|E_1|^2\,d\vec{r}$, which must exceed the threshold value $\sigma_1P_{\rm NLS}/\gamma_{11}$, where $P_{\rm NLS}=11.69$ is the power of the ground-state solitary wave solution to the standard (unit coefficients) 2D NLS equation (see [4] for a review).

In the opposite limit with infinitely many components, $N\rightarrow\infty$, Eqs. (1) can describe the propagation and self-focusing of partially incoherent light beams in noninstantaneous nonlinear media such as biased photorefractive materials [5]. Even though the photorefractive materials are noncentrosymmetric, and thus quadratic nonlinear, their nonlinearity in the direction of the bias field can be approximated under strong bias conditions by the cubic Kerr nonlinearity for broad low intensity beams. The possible existence of spatially incoherent solitary waves has been the subject of considerable interest since first observed in 1996 [6]. In contrast to their coherent counterparts, which normally require gigawatt laser pulses, the incoherent solitons can be excited by white light and require as little as milliwatts or even nano-

watts [7]. Due to the nature of the photorefractive nonlinearity, the theoretical studies of incoherent solitary waves have so far been concentrated on 1D models.

Here we are interested in the incoherent coupling between two waves, $N=2$, where Eqs. (1) can describe several different physical situations. In nonlinear optics the most well-known applications are to cubic nonlinear media, where they describe the nonresonant interaction between two orthogonally polarized waves with the same frequency [8] or two waves with the same polarization, but different frequencies (see, e.g., [1]). Furthermore, they describe the resonant interaction of a fundamental wave and its second harmonic in noncentrosymmetric crystals with both a quadratic and a cubic nonlinearity, in the limit when the interaction is far from being phase-matched (see, e.g., [9]).

In plasma physics the system (1) for $N=2$ can, for example, describe the so-called beat-wave accelerator [10], in which a large-amplitude Langmuir wave is generated by the beating of two laser beams, whose frequencies differ by approximately the plasma frequency. The longitudinal electrical field of this Langmuir wave can then be used to accelerate particles. The focusing Kerr nonlinearity of this system originates from the relativistic correction to the mass of the particles oscillating in the strong Langmuir field [10].

In the context of incoherent solitons, a thorough study of the fully 2D system (1) for $N=2$ is a first step on the way to a detailed understanding of the limit $N\rightarrow\infty$, which can describe incoherent self-focusing.

As for $N=1$ (the NLS equation), the system (1) can also be integrable for $N=2$ in 1D, but only for the specific symmetric case when $\sigma_n=\sigma$ and $\gamma_{jn}=\gamma$, i.e., when the diffraction and nonlinearity parameters are identical, respectively [11]. These coupled bright Manakov solitons were first observed experimentally in 1996 in $Al_xGa_{1-x}As$ planar waveguides, due to the difficulty in making the interaction completely incoherent, i.e., eliminating the four-wave-mixing terms [12].

The system (1) with $N=2$ has been abundantly studied in 1D since first derived in 1970 (see, e.g., [13]). Here we consider the 2D case, for which much less is known. One of the earliest studies was by McKinstrie and Russel in the context of the beat-wave accelerator [10]. They derived the so-called virial relation for general *N*-component initial conditions. For superimposed Gaussian waves, virial arguments showed that a negative Hamiltonian was a *sufficient* condition for collapse, corresponding to the fact that the total power must be above a certain threshold value. This was confirmed numerically [10].

The results for superimposed waves were recently extended to arbitrary dimensions, as part of a study of resonant interaction in quadratic nonlinear media [14]. In particular, in 2D, a *sufficient* condition for the absence of collapse was derived, requiring that the power in both components is below a certain threshold value. We note that this power threshold for the absence of collapse is generally lower than the threshold for occurrence of collapse found by McKinstrie and Russel.

McKinstrie and Russel also studied the so-called entrainment effect, in which two initially separated beams fuse before collapsing or diffracting as one entity [10]. In the particular case of symmetric positive coefficients ($\sigma_n=\frac{1}{2}, \gamma_{12}=\gamma_{21}=2\gamma_{nn}=\frac{1}{4}$) and two initially separated identical Gaussian waves, they used the virial relation to show that the waves could fuse and collapse as a single entity whenever their separation was below a certain threshold value and the total power was in between the threshold for collapse of two superimposed waves and of two waves infinitely far apart, where the system reduces to simply two uncoupled NLS equations. A numerical example with the separation slightly below (above) the threshold confirmed that the two waves fused before collapsing (diffracting) as one entity.

We note that the mechanism of fusion and subsequent collapse of two beams can also be found in the single-component NLS equation [15]. However, in this case the relative phase of the two beams plays a crucial role (i.e., two beams being π out of phase can never fuse), whereas the dynamics naturally is phase-independent when the interaction is incoherent as in Eqs. (1).

The results for initially separated waves were recently extended to arbitrary many components in [16]. Here virial theory and the internal structure of the Hamiltonian were used to further divide the collapse region ($H<0$) into two subregions, in which two Gaussian beams will collapse independently (i.e., never fuse) and fuse before collapsing, respectively. Variational calculations further predicted that initially close Gaussian beams with medium powers could oscillate about the center of mass and cross several times before eventually collapsing or diffracting [16]. The oscillations in the separation were found to be damped in the collapse regime, whereas they were increasing in amplitude in the diffraction regime.

In spite of the investigation performed by McKinstrie and Russel [10] and later by Bergé *et al.* [14,16], the spectrum of dynamical scenarios in incoherent two-wave interaction described by Eqs. (1) is so rich that several points still need to be investigated.

First, the possibility of realizing stable solitonlike states in a 2D system (bulk medium) is of considerable interest, since it may open up possibilities for all-optical switching applications. So, it is worth identifying the stationary bound states of Eqs. (1) and investigating their stability. In this respect it was recently predicted that the so-called ground states, defined as localized stationary waves minimizing the Hamiltonian, are stable in 1D [17] (see also [18]). In this case, as for solitons of the scalar NLS equation, the derivative of the power with respect to the soliton eigenvalue is positive [19]. However, in 2D the same derivative is zero and this criterion only predicts so-called marginal stability of the solitary waves [16]. Although such a theoretical result can suggest instability, numerical investigations of the existence and stability properties of the different solitary wave solutions are necessary.

Furthermore, it is worth verifying numerically the sufficient conditions for collapse and spreading of superimposed waves predicted theoretically in [10,14]. An important issue is whether the corresponding power thresholds are accurate measures of the actual power threshold for collapse. As we will show, this is only the case for identical initial conditions and symmetrical system parameters ($\sigma_1=\sigma_2$, $\gamma_{11}=\gamma_{22}$, $\gamma_{12}=\gamma_{21}$). In the highly asymmetrical case, collapse can still occur for positive Hamiltonians, which is in sharp

contrast to what is known from the NLS equation. We note that the examples presented in [10,16] were all for symmetrical cases.

Finally, although the process of fusion has already been predicted theoretically and confirmed numerically in [10], this was for initial separations well below the diameter of the individual wave. Clear examples of fusion when the components are well-separated still remain to be shown. Furthermore, a complete map of the different possible scenarios still remains to be given theoretically and confirmed numerically. For instance, it should be possible to separate the diffraction regime into coupled and independent behavior also, and it seems plausible that the two components may be able to oscillate about the center of mass and cross more than once before fusing, both in the collapse and diffraction regime. The latter was predicted from variational calculations in [16], but given the limitations of the variational approach, it needs to be confirmed numerically, i.e., are the oscillations really increasing in amplitude in the diffraction regime, or is it an artifact of the fixed test function?

In this paper we recall the conservation laws for localized solutions of Eqs. (1) for $N=2$ and $\sigma_1=\sigma_2$ in Sec. II. We derive sufficient criteria for collapse and spreading from a virial relation governing the mean-square radius of the total field in Sec. III. In Sec. IV, we find the different stationary solitary wave solutions and investigate their stability properties, both numerically and analytically. In Sec. V A we confirm the sufficient criteria numerically and show that only in the symmetrical case do they coincide and give a good approximation to the actual threshold. Finally, in Sec. V B, we consider the symmetrical case and use the internal structure of the Hamiltonian to analytically identify all four types of scenarios: independent collapse or spreading and fusion with subsequent collapse or spreading. To do so we introduce auxiliary parameters defining the degree of spatial overlap necessary for coupled behavior. The predictions are confirmed numerically and examples of damped oscillations before fusion are given in both the collapse and diffraction regimes.

II. THE MODEL

We consider two incoherently coupled waves propagating in a bulk Kerr medium, for which $\sigma_1=\sigma_2$ (corresponding to the case considered by McKinstrie and Russell [10]). In this case the equations given in the Introduction can, by means of a proper scaling, be written in the form

$$i\partial_z E_1+\nabla^2 E_1+(\eta_1|E_1|^2+\rho|E_2|^2)E_1=0, \tag{2}$$

$$i\partial_z E_2+\nabla^2 E_2+(\eta_2|E_2|^2+\rho|E_1|^2)E_2=0, \tag{3}$$

where $E_n=E_n(\vec{r},z)$ is the normalized slowly varying complex envelope function of the mode $n=1,2$, z is the propagation coordinate, $\vec{r}=(x,y)$, and $\rho=\pm 1$. In the following we will only consider positive SPM coefficients, $\eta_n>0$.

For periodic or sufficiently localized solutions, Eqs. (2) and (3) conserve the power $P_n=P_n(E_n)$ of each mode,

$$P_n(E_n)=\int |E_n|^2\, d\vec{r}, \tag{4}$$

the Hamiltonian $H=H(E_n)$,

$$H(E_n)=\int\left[|\nabla E_1|^2+|\nabla E_2|^2-\frac{\eta_1}{2}|E_1|^4-\frac{\eta_2}{2}|E_2|^4-\rho|E_1E_2|^2\right]d\vec{r}, \tag{5}$$

and the momentum $\vec{M}=\vec{M}(E_n)$,

$$\vec{M}(E_n)=2\int \mathrm{Im}\{E_1^*\nabla E_1+E_2^*\nabla E_2\}d\vec{r}. \tag{6}$$

Here we have defined the integral $\int d\vec{r}=\int\int dx\,dy$. Furthermore, Eqs. (2) and (3) are Hamiltonian and can be written as Hamilton's equations $i\partial_z E_n=\delta\mathcal{H}/\delta E_n^*$, where $\mathcal{H}$ is the Hamiltonian density, $H=\int\mathcal{H}\,d\vec{r}$, and $\delta/\delta E_n$ denotes the functional derivative with respect to E_n.

III. VIRIAL THEORY

Consider the beam width (mean-square radius) or so-called virial, $I(z)$, which we define as

$$I(z)=\frac{1}{P}\int R^2(|E_1|^2+|E_2|^2)d\vec{r}, \tag{7}$$

where $P=P_1+P_2$ is the total power, $\vec{R}=\vec{r}-\langle\vec{r}\rangle$, and $R^2=|\vec{R}|^2$. The total center of mass $\langle\vec{r}\rangle$ is defined as

$$\langle\vec{r}\rangle=\frac{1}{P}\int \vec{r}(|E_1|^2+|E_2|^2)\,d\vec{r} \tag{8}$$

and is easily found to obey the relation

$$\frac{d\langle\vec{r}\rangle}{dz}=\frac{\vec{M}}{P}\Rightarrow\frac{d^2\langle\vec{r}\rangle}{dz^2}=0. \tag{9}$$

Thus, for initial conditions with zero momentum, as we will use here, the center of mass is fixed. For periodic or sufficiently localized solutions to Eqs. (2) and (3), the virial satisfies the relation [14]

$$\frac{d^2I}{dz^2}=\frac{8H}{P}-\frac{2M^2}{P^2}, \tag{10}$$

where $M^2=|\vec{M}|^2$. If the right-hand side of Eq. (10) is negative, the beam width $I(z)$ will continuously decrease and a collapse, defined as $I(z)\to 0$, will inevitably occur at a finite distance. Thus $H-M^2/(4P)<0$ is a *sufficient condition* for collapse (since P is positive definite).

If the right-hand side of Eq. (10) is positive, $H-M^2/(4P)>0$, we have to do further analysis to determine whether a collapse can occur or not. For example, if the wave is given a sufficiently strong prefocusing at the input $[dI(0)/dz<0]$, a collapse could in principle develop despite the second derivative of the virial being constant and positive.

First we note that a collapse of the total wave function, $I(z)=I_1(z)+I_2(z)\to 0$, implies that each individual compo-

nent also collapses, $I_n(z)\to 0$ (since I_n is positive definite). Here $I_n(z)=P^{-1}\|RE_n\|_2^2$, with the standard L^p norm being given by

$$\|E_n\|_p=\left(\int |E_n|^p\, d\vec{r}\right)^{1/p}. \tag{11}$$

Conservation of P_n and the 2D bound

$$\|E_n\|_2^4\leqslant\|\nabla E_n\|_2^2\|RE_n\|_2^2, \tag{12}$$

further implies that the gradient norm goes to infinity, $\|\nabla E_n\|_2^2\to\infty$, when $I_n(z)\to 0$. Note that the adverse is not true, i.e., $\|\nabla E_n\|_2^2\to\infty$ does not imply that $I_n(z)\to 0$. Thus a singularity, in which the gradient norm diverges, can in principle develop despite the virial being finite.

To derive a more useful criterion in terms of the power, we use the Schwarz inequality $\|E_1E_2\|_2^2\leqslant\|E_1\|_4^2\|E_2\|_4^2$ and the Sobolev inequality $\|E_n\|_4^4\leqslant C\|\nabla E_n\|_2^2\|E_n\|_2^2$. The Sobolev inequality is optimized by the best constant $C=C_{\rm best}=2/P_{\rm NLS}$ [20], where $P_{\rm NLS}=11.69$ is the power of the ground-state solution of $\nabla^2E-E+E^3=0$, which can be found numerically [20]. Furthermore, we use Eq. (12) to connect the total power and virial,

$$P\leqslant 2I(\|\nabla E_1\|_2^2+\|\nabla E_1\|_2^2). \tag{13}$$

For $\rho\geqslant 0$ and $\eta_n\geqslant-\rho$ we can then bound the Hamiltonian (5) from below as follows:

$$H\geqslant\sum_{n=1}^{2}\left(1-\frac{P_n}{P_n^{\rm th}}\right)\|\nabla E_n\|_2^2. \tag{14}$$

If the individual powers are both below threshold,

$$P_n<P_n^{\rm th}\equiv\frac{P_{\rm NLS}}{\eta_n+\rho}, \tag{15}$$

then H and all coefficients in the sum (14) are positive, and we can use Eqs. (13) and (14) to bound d^2I/dz^2 as follows:

$$\frac{d^2I}{dz^2}\geqslant a_1+\frac{a_2}{I}, \tag{16}$$

where the constants $a_{1,2}$ are given by

$$a_1=-2M^2/P^2\leqslant 0,$$

$$a_2=4\,\min\{(1-P_1/P_1^{\rm th}),(1-P_2/P_2^{\rm th})\}>0.$$

It is straightforward to do an integration of Eq. (16) and show that collapse is only possible if $a_2<0$ (see [14] for details).

Since $a_2>0$ (and $H>0$) always when both individual powers are below threshold, collapse cannot occur in this case. In fact, from Eq. (14) and the conservation of (a finite) H, it follows that any singularity, in which the gradient norm goes to infinity, cannot occur when Eq. (15) is fulfilled for both components. Thus $P_n<P_n^{\rm th}$ is a *sufficient condition* for the absence of collapse. In this low-power case the beam will eventually spread out with $I(z)\to\infty$.

In the case when at least one of the components has a power above threshold, the bound (14) does not forbid collapsing solutions with $I_n(z)\to 0$, or any singularities with $\|\nabla E_n\|_2^2\to\infty$, regardless of the sign of H and the right-hand side of Eq. (10), and regardless of the sign and strength of the initial gradient $dI(0)/dz$. This interesting property, which is due to the multicomponent nature of the system (2) and (3), will be demonstrated numerically in the following, where we also confirm the sufficient conditions $H-M^2/(4P)<0$ for collapse and $P_n<P_n^{\rm th}$ for spreading.

The virial relation for Eqs. (1) with arbitrarily many coupled equations was first developed by McKinstrie and Russel [10] and later by Bergé [16]. The rigorous proof of the absence of collapse for $\rho\geqslant 0$ and $\eta_n+\rho\geqslant 0$ in the system of two coupled Eqs. (2) and (3) when the individual powers are below threshold was first given in [14], and later for an arbitrary number of equations in [16]. Here we have just given the main steps.

Before proceeding, we would like to point out two important things to be aware of. First, the application of the Schwarz inequality $\|E_1E_2\|_2^2\leqslant\|E_1\|_4^2\|E_2\|_4^2$ in deriving the bound (14) means that any information on the effect of an initial separation between the two components is lost, and that $P_n^{\rm th}$ can significantly underestimate the actual power threshold for large separations. Thus virial theory only gives information about an initial separation through the sufficient criterion for collapse, $H-M^2/(4P)<0$.

Second, the virial theory predicts whether or not a global collapse of the wave function into a single point will occur over a finite distance, in which all the power becomes focused at that point with the amplitude going to infinity (i.e., the virial goes to zero and, due to conservation of power, the gradient norm goes to infinity). Typically such a collapse is preceded by a so-called blow-up, in which the amplitude locally goes to infinity, and the solution ceases to exist, while the power can still be arbitrarily distributed (i.e., the gradient norm goes to infinity while the virial remains finite).

This is, e.g., a well-known property of solutions to the NLS equation in two or more transverse dimensions (see [4]). For the critical 2D NLS equation it is further well-established numerically that the singularity captures exactly the power $P_{\rm NLS}$ of the ground-state solitary wave solution, and that it locally has a self-similar structure (see, e.g., [21,22]).

In this work we are mainly interested in the threshold for the development of a (collapse) singularity, and not so much in what the specific profile looks like at this singularity. In the following we will therefore not distinguish between a collapse and a blow-up, but use the term collapse for both scenarios.

IV. BRIGHT SOLITARY WAVES

The system (2) and (3) are invariant under the scaling

$$E_n\hookrightarrow\lambda E_n,\quad \vec{r}\hookrightarrow\lambda\vec{r},\quad z\hookrightarrow\lambda^2 z. \tag{17}$$

Keeping this in mind, we consider stationary exponentially localized bright solitary wave solutions (with no nodes, i.e., lowest-order bound states) of the form

$$E_n(\vec{r},z)=\lambda\psi_n(\xi)e^{i\lambda^2 z},\quad \xi=\lambda r,\quad r=|\vec{r}|, \tag{18}$$

where the soliton eigenvalue λ is real and the real and symmetric functions ψ_n decay monotonically to zero as ξ increases. Inserting the solution (18) into Eqs. (2) and (3), we obtain the stationary equations

$$\ddot{\psi}_1+\xi^{-1}\dot{\psi}_1-\psi_1+(\eta_1\psi_1^2+\rho\psi_2^2)\psi_1=0, \tag{19}$$

$$\ddot{\psi}_2+\xi^{-1}\dot{\psi}_2-\psi_2+(\eta_2\psi_2^2+\rho\psi_1^2)\psi_2=0, \tag{20}$$

where a dot denotes differentiation with respect to ξ.

The individual and total power of the solutions (18) are independent of the solution parameter λ, i.e., $P(E_n)=P(\psi_n)$ or $dP(E_n)/d\lambda=0$. Thus the solutions are so-called marginally stable according to the Vakhitov-Kolokolov (VK) criterion, which requires $dP/d\lambda>0$ ($dP/d\lambda<0$) for stability (instability) [19]. However, in contrast to the NLS equation, the VK criterion for stability is only a *necessary criterion* in this system of coupled NLS equations [16]. The proof of it being also a sufficient criterion is still an open problem and certainly nontrivial. In media with both quadratic and cubic nonlinearity, examples have been given in which the VK criterion fails and predicts stability of solutions that numerical simulations show to be unstable [23].

Multiplying Eqs. (19) and (20) with ψ_1 and ψ_2, respectively, and integrating the sum, it is straightforward to obtain the relation $P_s=\|\nabla\psi_1\|_2^2+\|\nabla\psi_2\|_2^2-2H_s$, where $P_s=P_1(\psi_1)+P_2(\psi_2)$ and $H_s=H(\psi_n)$ are the total power and Hamiltonian evaluated on the soliton solutions (18). Doing the same with $\vec{R}\cdot\nabla\psi_n$, one can obtain the relation $P_s=\|\nabla\psi_1\|_2^2+\|\nabla\psi_2\|_2^2-H_s$. Combining these two relations, we see that the Hamiltonian is zero on the soliton solutions, $H_s=0$. Furthermore, the soliton solutions (18) have zero momentum, $\vec{M}_s=\vec{M}(\psi_n)=(0,0)$, which means that the center of mass is constant, $d\langle\vec{r}\rangle/dz=\vec{0}$, and that $dI(0)/dz=0$. Therefore the virial relation, $d^2I/dz^2=0$, predicts correctly that the width of the solitons also remains constant, $I(z)=I(0)$.

From the above we would expect that the soliton solutions (18) are unstable, as is the case for the stationary solutions to the 2D NLS equation, which have the same characteristics: $dP_s/d\lambda=0$, $H_s=0$, and $I(z)=I(0)$. Thus we expect that there are no stable states towards which the Gaussian initial conditions that we consider in the following sections can evolve. For completeness, we will nevertheless briefly consider the regimes of the existence of the soliton solutions (18).

The bright solitary wave solutions (18) can be categorized into three types, the C, W, and V solutions, borrowing the notation from systems with both $\chi^{(2)}$ and $\chi^{(3)}$ nonlinearities [24]: The C solution, where both components are nonzero, with no particular relative size, can generally only be found numerically. However, when $\eta_n>0$ and $\rho=\pm1$ fulfill one of the requirements

$$\begin{aligned}&\text{(I)}\quad \rho>\max\{\eta_1,\eta_2\},\\ &\text{(II)}\quad \rho<\min\{\eta_1,\eta_2\},\\ &\text{(III)}\quad \eta_1=\eta_2=\rho=1,\end{aligned} \tag{21}$$

then one C solution has the form

$$\psi_2(\xi)=\alpha\psi_1(\xi)=\frac{\alpha}{\sqrt{\eta_1+\rho\alpha^2}}\psi(\xi), \tag{22}$$

where the parameter α is given by

$$\alpha=\begin{cases}\sqrt{(\eta_1-\rho)/(\eta_2-\rho)} & \text{for I,II,}\\ \text{arbitrary} & \text{for III,}\end{cases} \tag{23}$$

and where $\psi(\xi)$ is the solution to the stationary nonlinear Schrödinger (NLS) equation

$$\ddot{\psi}+\xi^{-1}\dot{\psi}-\psi+\psi^3=0. \tag{24}$$

The partial powers of this C solution are therefore $P_2^{\mathrm{c}}=\alpha^2P_1^{\mathrm{c}}=\alpha^2P_{\mathrm{NLS}}/(\eta_1+\rho\alpha^2)$. An analytical expression for the solution to the 2D NLS equation is not known, but a good approximation can be found by variational techniques to be [25]

$$\psi(\xi)=A_0\,\mathrm{sech}(B_0\xi), \tag{25}$$

where $A_0^2=12\ln2/(4\ln2-1)$ and $B_0^2=6\ln2/(2\ln2+1)$.

In the particular case when $\eta_1=\eta_2$ (giving $\alpha=1$), the partial powers of the C solution are identical to the threshold powers found by virial theory, $P_n^{\mathrm{c}}=P_n^{\mathrm{th}}=P_{\mathrm{NLS}}/(\eta_n+\rho)$. In the general case when $\eta_1\neq\eta_2$, the two are different.

The single-component W solution exists for all $\eta_1>0$. It has $\psi_2=0$ and ψ_1 is the solution to the stationary NLS equation

$$\ddot{\psi}_1+\xi^{-1}\dot{\psi}_1-\psi_1+\eta_1\psi_1^3=0. \tag{26}$$

Thus the W solution has the power $P^{\mathrm{w}}=P_1^{\mathrm{w}}=P_{\mathrm{NLS}}/\eta_1$, and is approximately given by

$$\psi_1(\xi)=A_0\sqrt{1/\eta_1}\,\mathrm{sech}(B_0\xi). \tag{27}$$

The single-component V solution exists for all $\eta_2>0$. It has $\psi_1=0$ and ψ_2 is the solution to the stationary NLS equation

$$\ddot{\psi}_2+\xi^{-1}\dot{\psi}_2-\psi_2+\eta_2\psi_2^3=0. \tag{28}$$

Thus the V solution has the power $P^{\mathrm{v}}=P_2^{\mathrm{v}}=P_{\mathrm{NLS}}/\eta_2$ and is approximately given by

$$\psi_2(\xi)=A_0\sqrt{1/\eta_2}\,\mathrm{sech}(B_0\xi). \tag{29}$$

Note that the C solutions can also exist for negative values of the SPM coefficients η_n, whereas this is not the case for the W and V solutions.

We have numerically found the families of C, W, and V solutions using a standard relaxation technique. In Fig. 1 we show the individual powers P_n versus the SPM coefficient $\eta_2>0$ for $\eta_1=4$ and $\rho=1$. From the requirement (21) we expect that the C solutions exist for $\eta_2>1$, while the W and V solutions exist for all $\eta_2>0$. Furthermore, at $\eta_1=\eta_2$, where $\alpha=1$, the partial power for the C solution should be

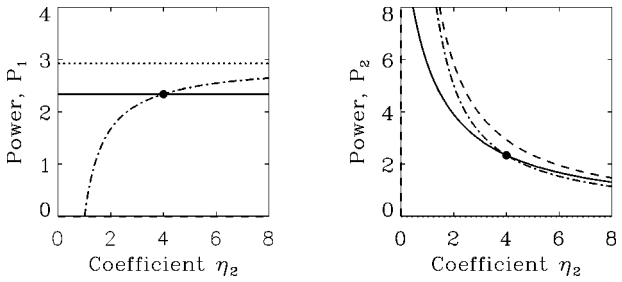

FIG. 1. Individual power P_1 (left) and P_2 (right) versus η_2 for the C (dash-dotted), W (dotted), and V solutions (dashed) of Eqs. (19) and (20), with $\eta_1=4$ and $\rho=1$. The solid curve indicates the corresponding threshold power $P_n^{\rm th}$.

equal to the corresponding threshold power for collapse, $P_n^{\rm c}=P_n^{\rm th}=P_{\rm NLS}/(\eta_1+\rho)$. The numerical results confirm that this is true, and that the predicted partial powers of the three types of solutions are correct.

Using an iterative, radially symmetric, midpoint Crank-Nicholson finite difference scheme, we have performed numerical simulations of Eqs. (2) and (3) with the C, W, and V solutions as initial conditions. We used a resolution of $dr=10^{-3}$ over the interval $r=[0,40]$ and a stepsize of $dz=10^{-3}$. In all test cases ($\rho=1$, $\eta_1=4$, and $\eta_2=3,4,5$) all three types of solitary waves were observed to be unstable, with the perturbation introduced by the discrete numerical sampling causing the center amplitude to blow up after a finite propagation distance, just as for the critical NLS equation [26]. Although this is not a proof, it suggests that solitary waves of the form (18) are unstable for positive coefficients $\eta_n>0$ and $\rho=1$ [see discussion below Eq. (20)].

V. COLLAPSE IN 2D

A. Both components with the same center

In this section we numerically investigate the threshold power for collapse, and the different possible dynamical scenarios with Gaussian initial conditions of the form

$$E_n(\vec{r},0)=\sqrt{\frac{P_n}{\pi\Delta^2}}\exp\left(-\frac{r^2}{2\Delta^2}\right), \tag{30}$$

where both components are centered at the origin. In this case $M=dI(0)/dz=0$ and thus the virial relation (10) reduces to $dI^2/dz^2=8H/P$, where the Hamiltonian can be calculated explicitly to

$$H=\sum_{n=1}^{2}\frac{P_n}{\Delta^2}\left(1-\frac{\eta_n P_n+\rho P_{3-n}}{4\pi}\right). \tag{31}$$

A *sufficient condition* for collapse of the solution to Eqs. (2) and (3) with initial condition (30) is therefore $H<0$. Introducing the ratio $\beta=P_1/P_2$, which we typically fix in our numerical simulations, we can reduce H to

$$H=\frac{P}{\Delta^2}\left(1-\frac{P}{\mathcal{P}_{\rm up}^{\rm th}}\right), \tag{32}$$

where the threshold power $\mathcal{P}_{\rm up}^{\rm th}$ is given by

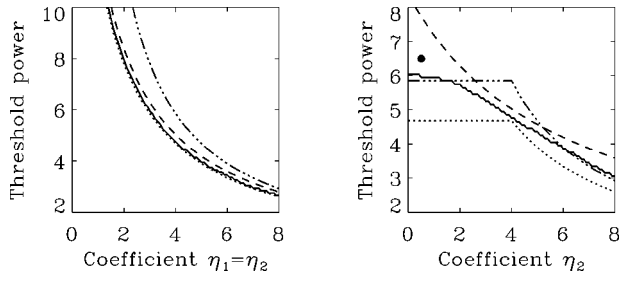

FIG. 2. Threshold power versus $\eta_1=\eta_2$ (left) and η_2 (right) for $\eta_1=4$. Solid lines represent numerical results and dotted and dashed lines represent the virial predictions (34) and (35), respectively. The dash-dotted lines represent the prediction $\min\{2P_{\rm NLS}/\eta_1,2P_{\rm NLS}/\eta_2\}$. The initial condition is Eq. (30) with $P_1=P_2$, $\Delta=2$, and $\rho=1$. The filled circle marks a case for which we show the specific evolution in Fig. 3.

$$\mathcal{P}_{\rm up}^{\rm th}=\frac{(1+\beta)^2P_{\rm NLS}^{\rm Gaus}}{\beta^2\eta_1+\eta_2+2\beta\rho}. \tag{33}$$

From Eq. (32) we see that $H<0$ ($H>0$) corresponds to the total power being above (below) the threshold $\mathcal{P}_{\rm up}^{\rm th}$. Here $P_{\rm NLS}^{\rm Gaus}=4\pi$ corresponds to the power of the Gaussian approximation to the ground-state solution to the 2D NLS Eq. (24), which can be obtained by variational techniques. For $\beta=0$ ($\beta=\infty$) we recover the threshold power $4\pi/\eta_2$ ($4\pi/\eta_1$) for collapse of a Gaussian initial condition in the 2D NLS equation.

We have performed numerical simulations of the dynamical Eqs. (2) and (3) using the Crank-Nicholson routine described in Sec. IV, and the initial condition (30) with $P_1=P_2=P/2$, $\Delta=2$, and $\rho=1$. The resolution was $dr=10^{-3}$ over the interval $r=[0,30]$ and the stepsize was $dz=10^{-2}$. When the beams diffract this keeps the relative deviations of both P and H from their respective initial values below 10^{-6} over a distance $z=[0,50]$.

For this particular case, the sufficient conditions predicted from virial theory, which can be obtained from Eqs. (15), (32) and (33), reduce to

$$\text{No collapse:}\quad P<\mathcal{P}_{\rm low}^{\rm th}=\min\left\{\frac{2P_{\rm NLS}}{\rho+\eta_1},\frac{2P_{\rm NLS}}{\rho+\eta_2}\right\}, \tag{34}$$

$$\text{Collapse:}\quad P>\mathcal{P}_{\rm up}^{\rm th}=\frac{2P_{\rm NLS}^{\rm Gaus}}{\rho+(\eta_1+\eta_2)/2}, \tag{35}$$

where Eq. (34) is only valid for $\rho\geqslant 0$ and $\eta_n\geqslant-\rho$. Thus for low powers fulfilling Eq. (34) the beam will spread out with $I(z)\to\infty$. For high powers fulfilling Eq. (35) the beam will collapse at a finite distance.

In Fig. 2 we show the numerically found threshold power, above which the solution collapses at the center at a finite distance $Z_{\rm coll}<50$. As the collapse is approached, the evolution in z becomes so fast that the numerical routine with fixed stepsize no longer conserves P. As a convenient and reliable definition we therefore detect a collapse as when the relative deviation of P from its initial value has increased to more than 10^{-4}.

For the symmetrical case (left figure) when $\eta_1=\eta_2$ and $P_1=P_2$ the lower and upper thresholds become formerly

identical, within the approximation $P_{\rm NLS}^{\rm Gaus} \approx P_{\rm NLS}$. In this case we see that the numerically calculated threshold power (solid curve) lies exactly on top of the lower threshold $\mathcal{P}_{\rm low}^{\rm th} = 2P_{\rm NLS}/(\eta_2+\rho)$ (dotted curve). For $P<\mathcal{P}_{\rm low}^{\rm th}$ we always observed that both components spread out with $I_n(z)\to\infty$. Thus the numerical results confirm that Eqs. (34) and (35) are sufficient conditions for spreading and collapse, respectively. Note that with the resolution $dr=10^{-3}$ the effect of discreteness, which tends to lower the threshold power [26], can be neglected.

In the right side of Fig. 2 we show the threshold of collapse versus η_2 when $\eta_1=4$ is fixed and $P_1=P_2$. We see that when the asymmetry is weak, $\eta_2 \approx \eta_1$, the numerically calculated threshold is close to the predictions (34) and (35), which in turn are close to each other. When the asymmetry becomes pronounced, i.e., when η_2 and η_1 are significantly different, the gap between $\mathcal{P}_{\rm low}^{\rm th}$ and $\mathcal{P}_{\rm up}^{\rm th}$ widens and we see that the actual threshold lies in between the two limits. However, the predictions (34) and (35) are never violated, and thus the numerical results also confirm the virial predictions in this more complicated asymmetrical case.

In the highly asymmetric limit when $\eta_1 \gg \eta_2$ or $\eta_1 \ll \eta_2$, we can obtain a good approximation to the actual collapse threshold from heuristical arguments: Take the example with $\eta_1 \gg \eta_2$ and identical initial conditions for the two components, $P_1=P_2$. Assume that we can disregard the XPM term that couples the two modes together. In that case the power threshold of the component E_n is simply $P_{\rm NLS}/\eta_n$, as in the conventional 2D NLS equation, and thus the threshold in the total power is $2P_{\rm NLS}/\eta_n$. Assume now that E_1 is collapsing ($P_1>P_{\rm NLS}/\eta_1$) and that E_2 is diffracting rapidly ($P_2 \ll P_{\rm NLS}/\eta_2$). Then, even in the presence of the XPM terms, the collapse dynamics will be primarily driven by the E_1 component and as a first approximation we can disregard the rapidly decreasing influence of the diffracting E_2 component. Since the power in each component individually is conserved, the presence of the other (diffracting) beam in the equation for a given component through the XPM term simply adds a focusing potential (for $\rho>0$), which acts as a waveguide, and tries to keep the beam focused. This should merely decrease the collapse threshold slightly.

According to these arguments, the actual threshold will be close to $\min\{2P_{\rm NLS}/\eta_1, 2P_{\rm NLS}/\eta_2\}$ in the highly asymmetrical limits when $\eta_1 \gg \eta_2$ or $\eta_1 \ll \eta_2$, and of course also when the XPM term can be neglected, i.e., when $\eta_1 \gg \rho$ and $\eta_2 \gg \rho$. Away from these limits the threshold should be somewhat lower than $\min\{2P_{\rm NLS}/\eta_1, 2P_{\rm NLS}/\eta_2\}$. This is exactly what we observe in Fig. 2.

These numerical results highlight the interesting property of an asymmetric multicomponent system, such as Eqs. (2) and (3) for $\eta_1 \neq \eta_2$ and $P_1=P_2$, namely that collapse is possible even when the second derivative of the virial is always positive, $d^2I/dz^2 = 8H/P > 0$, i.e., when the total mean-square radius is always increasing. This effect cannot be observed in, e.g., the symmetric case or the NLS equation, where there is only one wave function that determines the dynamics.

To illustrate this, we show in Fig. 3 the evolution of the center amplitudes and the virial for the asymmetric case

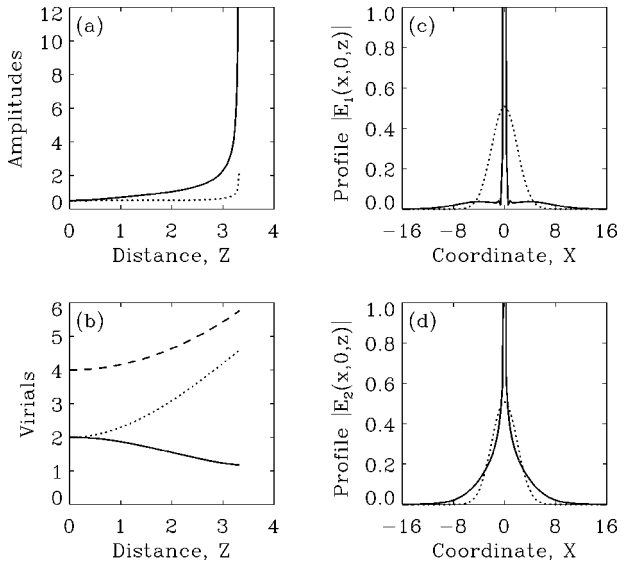

FIG. 3. Evolution of (a) the amplitudes $|E_n(0,0,z)|$ and (b) the virials $I_n(z)$ for the first (solid) and second (dotted) component. The total virial $I(z)$ is shown with a dashed line. (c) and (d): Profiles $|E_n(x,0,z)|$ at $z=0$ (dotted) and at collapse $z=4.77$ (solid). Results of numerical integration of Eqs. (2) and (3) for $\eta_1=8\,\eta_2=4$ and $P_1=P_2=3.25$, corresponding to the marked point in Fig. 2.

when $\eta_1=8\,\eta_2=4$ and $P=6.5$ ($H=0.13>0$ and $\mathcal{P}_{\rm low}^{\rm th}<P<\mathcal{P}_{\rm up}^{\rm th}$) marked by a filled circle in Fig. 2. In this case $P_1=3.25$ is above the NLS threshold $P_{\rm NLS}/\eta_1=2.92$, while $P_2=3.25$ is below the NLS threshold $P_{\rm NLS}/\eta_2=23.38$. As expected, the first component self-focuses [$I_1(z)$ decreases], while the second component spreads out [$I_2(z)$ increases]. In the end the first component ''pulls'' the center amplitude of the second component with it and a collapse singularity develops at $z=3.32$, in which the amplitude of both components diverges to infinity.

An equivalent discussion of collapse in media with both a $\chi^{(2)}$ and $\chi^{(3)}$ nonlinearity can be found in Refs. [14,27]. Here this effect of asymmetry on the collapse threshold in multicomponent systems was also observed.

B. Initially separated components

After having numerically confirmed the predictions of virial theory for initial conditions with both components centered at the origin, we now consider Gaussian initial conditions of the form

$$E_n(\vec{r},0) = \sqrt{\frac{P_n}{\pi\Delta^2}}\exp\left(-\frac{(x-x_n)^2+y^2}{2\Delta^2}\right), \qquad (36)$$

where the two components are located at a distance δ_0 away from each other, with $x_1=-x_2=\delta_0/2$. In this case the virial relation is still $d^2I/dz^2=8H/P$, since $M=dI(0)/dz=0$. The Hamiltonian still has the form (32), but now the upper power threshold depends on the initial separation,

$$\mathcal{P}_{\rm up}^{\rm th}(\delta_0) = \frac{4\pi(1+\beta)^2}{\beta^2\eta_1+\eta_2+2\beta\rho e^{-\delta_0^2/2\Delta^2}}. \qquad (37)$$

In contrast, the lower power threshold does not depend on the initial separation and is still given by Eq. (34). Thus $P > \mathcal{P}^{\rm th}_{\rm up}(\delta_0)$ $(H<0)$ is still a sufficient condition for collapse and (for $\rho \geqslant 0$ and $\eta_n \geqslant -\rho$) $P < \mathcal{P}^{\rm th}_{\rm low}$ is still a sufficient condition for spreading.

Introducing an initial separation of the two components means that the number of different dynamical scenarios increases significantly. McKinstrie and Russel used the virial relation to separate the (P,δ_0) space into regions of collapse $(H<0)$ and spreading $(H>0)$ [10]. A collapse implies per definition that the virial decreases until all the power becomes concentrated at one point after a finite distance. Thus, when the two components are initially separated, it means that they will attract and eventually fuse before collapsing as one entity. Fusion was observed numerically for $H<0$ where the components subsequently collapsed as one entity, and also for $H>0$ where they subsequently spread out as one entity [10]. Bergé recently used the internal structure of the Hamiltonian to separate the collapse regime into regions where the components collapse individually and where they fuse before collapsing [16].

However, as we have seen in the preceding section, $H=0$ is only an accurate measure of the collapse threshold in the nearly symmetric case when $\eta_1 \approx \eta_2$ and $P_1 \approx P_2$. When the asymmetry becomes pronounced, the gap between $\mathcal{P}^{\rm th}_{\rm up}$ and the actual threshold power widens, and collapse can occur well into the region where H is positive, as we have shown in Sec. V A. It is therefore important that the specific examples presented in [10,16] were exactly for the symmetric case when $\eta_1 = \eta_2$ and $P_1 = P_2$.

Our aim here is to analytically map out all possible scenarios in terms of the initial separation and power, and then confirm the predictions numerically. We will focus on the nearly symmetric case, where $\eta_1 \approx \eta_2$ and $P_1 \approx P_2$, and where we can compare directly with the results and examples of [10,16]. This simplifies the calculations considerably in that $H=(1-P/\mathcal{P}^{\rm th}_{\rm up})P/\Delta^2=0$ is a good measure of the actual threshold between collapse and diffraction. Thus $H<0$ $(P>\mathcal{P}^{\rm th})$ is a sufficient condition for collapse, and $H>0$ $(P<\mathcal{P}^{\rm th})$ is to a good approximation a sufficient condition for spreading. In other words, the Hamiltonian determines the dynamics of the system.

Note that in deriving $\mathcal{P}^{\rm th}_{\rm low}$ any dependence on the separation has been eliminated, as can be seen by comparing Eqs. (34) and (37) in the symmetric case. Thus, if $\mathcal{P}^{\rm th}_{\rm low}$ is to be an accurate measure of the actual collapse threshold, it requires not only that the system be nearly symmetric, but also that the separation δ_0 be much less than the width of the individual component Δ. Even so, we will not consider $\mathcal{P}^{\rm th}_{\rm low}$ in the theoretical analysis, since it gives no information about the effect of δ_0.

To determine the possible dynamics, we rewrite the Hamiltonian in the form $H(\delta_0)=H_{\rm free}+H_{\rm int}(\delta_0)$, where the free part $H_{\rm free}=H(\infty)$ is given by

$$H_{\rm free}=\frac{P^2}{\Delta^2}\left(\frac{1}{P}-\frac{1}{P^{\rm th}_\infty}\right) \tag{38}$$

and the interaction part $H_{\rm int}(\delta_0)$ is given by

$$H_{\rm int}(\delta_0)=\frac{P^2}{\Delta^2}\left(\frac{1}{P^{\rm th}_\infty}-\frac{1}{P^{\rm th}_0}\right)e^{-\delta_0^2/2\Delta^2}. \tag{39}$$

Here $\mathcal{P}^{\rm th}_0=\mathcal{P}^{\rm th}_{\rm up}(0)$ is the threshold when $\delta_0=0$ and the two components are superimposed, and $\mathcal{P}^{\rm th}_\infty=\mathcal{P}^{\rm th}_{\rm up}(\infty)$ is the threshold in the limit $\delta_0\to\infty$, where they are isolated from each other and evolve independently.

We will consider positive coefficients, $\eta_n>0$ and $\rho>0$, in which case $\mathcal{P}^{\rm th}_{\rm up}(\delta_0)$ increases with δ_0. Thus $\mathcal{P}^{\rm th}_0<\mathcal{P}^{\rm th}_\infty$ and $H_{\rm int}(\delta_0)$ is always negative. It is straightforward to extend the theory to negative coefficients as long as $\mathcal{P}^{\rm th}_{\rm up}(\delta_0)$ remains positive for all δ_0.

First we separate the (P,δ_0) space into regions of collapse and diffraction. For a given separation the threshold power that separates these two regions is given by $P=\mathcal{P}^{\rm th}_{\rm up}(\delta_0)$. For a given power in the range $\mathcal{P}^{\rm th}_0 \leqslant P \leqslant \mathcal{P}^{\rm th}_\infty$ we can define the corresponding threshold value of the initial separation, $\delta^{\rm th}_0$, from the relation $H_{\rm free}+H_{\rm int}(\delta^{\rm th}_0)=0$, which is equivalent to inverting Eq. (37). From Eqs. (38) and (39) we find $\delta^{\rm th}_0(P)$ to be

$$\frac{\delta^{\rm th}_0}{\Delta}=\sqrt{2\ln\left(\frac{1-\mathcal{P}^{\rm th}_\infty/\mathcal{P}^{\rm th}_0}{1-\mathcal{P}^{\rm th}_\infty/P}\right)}, \tag{40}$$

which is valid for $\mathcal{P}^{\rm th}_0 \leqslant P \leqslant \mathcal{P}^{\rm th}_\infty$. This threshold separation was first found in [10] for the symmetric case $\eta_1=\eta_2$ and $P_1=P_2$, and later in [16] for the general case.

By considering the internal structure of the Hamiltonian, we can further separate the collapse and diffraction regimes into each of their subregions of coupled and uncoupled behavior. Thus we can expect a strong interaction between the components when $|H_{\rm int}|$ is of the same order as $|H_{\rm free}|$ or larger, whereas the interaction will be negligible when $|H_{\rm int}| \ll |H_{\rm free}|$. This means that we can define a critical initial separation, for which $|H_{\rm int}|$ is some given fraction $\theta \leqslant 1$ of $|H_{\rm free}|$, and below which the interaction between the two components is strong enough for them to attract and merge at a finite distance.

From the definition $|H_{\rm int}(\delta^{\rm col}_0)/H_{\rm free}|=\theta_{\rm col}$ we find the critical separation in the collapse regime $\delta^{\rm col}_0$ to be

$$\frac{\delta^{\rm col}_0}{\Delta}=\sqrt{2\ln\left[-\frac{1}{\theta_{\rm col}}\left(\frac{1-\mathcal{P}^{\rm th}_\infty/\mathcal{P}^{\rm th}_0}{1-\mathcal{P}^{\rm th}_\infty/P}\right)\right]}, \tag{41}$$

which is valid for $\mathcal{P}^{\rm th}_\infty \leqslant P \leqslant \mathcal{P}_{\rm max}$. The upper limit $\mathcal{P}_{\rm max}$ is given by

$$\mathcal{P}_{\rm max}=\frac{\theta_{\rm col}\mathcal{P}^{\rm th}_0\mathcal{P}^{\rm th}_\infty}{(\theta_{\rm col}+1)\mathcal{P}^{\rm th}_0-\mathcal{P}^{\rm th}_\infty} \tag{42}$$

for $(\mathcal{P}^{\rm th}_\infty-\mathcal{P}^{\rm th}_0)/\mathcal{P}^{\rm th}_0<\theta_{\rm col}$, whereas $\mathcal{P}_{\rm max}=\infty$ when $(\mathcal{P}^{\rm th}_\infty-\mathcal{P}^{\rm th}_0)/\mathcal{P}^{\rm th}_0 \geqslant \theta_{\rm col}$. Similarly, from the definition $|H_{\rm int}(\delta^{\rm dif}_0)/H_{\rm free}|=\theta_{\rm dif}$ the critical separation in the diffraction regime $\delta^{\rm dif}_0$ becomes

$$\frac{\delta^{\rm dif}_0}{\Delta}=\sqrt{2\ln\left[\frac{1}{\theta_{\rm dif}}\left(\frac{1-\mathcal{P}^{\rm th}_\infty/\mathcal{P}^{\rm th}_0}{1-\mathcal{P}^{\rm th}_\infty/P}\right)\right]}, \tag{43}$$

which is valid for $\mathcal{P}_{\min} \leqslant P \leqslant \mathcal{P}_{\infty}^{\mathrm{th}}$. The lower limit $\mathcal{P}_{\min}$ is given by

$$\mathcal{P}_{\min} = \frac{\theta_{\mathrm{dif}} \mathcal{P}_0^{\mathrm{th}} \mathcal{P}_{\infty}^{\mathrm{th}}}{(\theta_{\mathrm{dif}} - 1)\mathcal{P}_0^{\mathrm{th}} + \mathcal{P}_{\infty}^{\mathrm{th}}}. \tag{44}$$

From the predictions of virial theory we can therefore identify the following regimes of different characteristic dynamics.

(I) When $|H_{\mathrm{int}}/H_{\mathrm{free}}| < \theta_{\mathrm{dif}}$ and $H > 0$, both components will spread out independently. This is the case for low powers $P < \mathcal{P}_{\infty}^{\mathrm{th}}$ when $\delta_0 > \delta_0^{\mathrm{dif}}$.

(II) When $|H_{\mathrm{int}}/H_{\mathrm{free}}| > \theta_{\mathrm{dif}}$ and $H > 0$, the components will interact strongly and merge at a finite distance before eventually spreading out. This requires low power $P < \mathcal{P}_{\infty}^{\mathrm{th}}$ and $\delta_0^{\mathrm{th}} < \delta_0 < \delta_0^{\mathrm{dif}}$.

(III) When $|H_{\mathrm{int}}/H_{\mathrm{free}}| > \theta_{\mathrm{col}}$ and $H < 0$, the components will interact strongly and merge before collapsing at a finite distance [with $I(z) \to 0$]. This is the case for low powers $P < \mathcal{P}_{\infty}^{\mathrm{th}}$ when $\delta_0 < \delta_0^{\mathrm{th}}$, and for high powers $P > \mathcal{P}_{\infty}^{\mathrm{th}}$ when $\delta_0 < \delta_0^{\mathrm{col}}$.

(IV) When $|H_{\mathrm{int}}/H_{\mathrm{free}}| < \theta_{\mathrm{col}}$ and $H < 0$, the components will collapse independently at a finite distance. This requires high power $P > \mathcal{P}_{\infty}^{\mathrm{th}}$ and $\delta_0 > \delta_0^{\mathrm{col}}$.

We have distinguished here between the fraction necessary for strong interaction in the low-power ($P < \mathcal{P}_{\infty}^{\mathrm{th}}$) diffraction regime, θ_{dif}, and the high-power ($P > \mathcal{P}_{\infty}^{\mathrm{th}}$) collapse regime, θ_{col}.

Collapse is a violent effect generally taking place over a relatively short distance, whereas the components can have a much longer interaction length when diffracting. It is therefore natural to expect that the initial overlap in the collapse regime, quantified by θ_{col}, should be larger than the initial overlap in the diffraction regime, θ_{dif}, in order for the waves to fuse before having collapsed or diffracted. Furthermore, the interaction, or overlap, will increase when the beams diffract individually, even without the XPM. In contrast, an individual collapse of the beams will decrease the beam size and thus tend to decrease the overlap. A reasonable conjecture would therefore be that $\theta_{\mathrm{col}} \approx 1$, whereas $\theta_{\mathrm{dif}} < 0.5$. However, the specific values of these fractions must be determined numerically.

Note that $\delta_0^{\mathrm{th}} = \delta_0^{\mathrm{dif}}$ when $\theta_{\mathrm{dif}} = 1$. In this case the theory would predict that regime II with strongly coupled but diffractive behavior is absent. In the particular degenerate case when $\theta_{\mathrm{dif}} = \theta_{\mathrm{col}} = 1$, the expressions for all the characteristic separations δ_0^{th}, δ_0^{dif}, and δ_0^{col} could be combined into one, corresponding to Eq. (40) with the parentheses replaced by a numerical value sign.

The approach of using the internal structure of the Hamiltonian to characterize the dynamics was first applied in [16], but without specifically introducing the additional degrees of freedom θ_{dif} and θ_{col}. Instead $|H_{\mathrm{int}}| = |H_{\mathrm{free}}|$ was assumed to give the critical separation, which we see corresponds to the degenerate case $\theta_{\mathrm{dif}} = \theta_{\mathrm{col}} = 1$. Furthermore, the existence of the cutoff $\mathcal{P}_{\max}$ has not been investigated yet.

Thus the separation of the diffraction region into the two regimes I and II, which originates from $\theta_{\mathrm{dif}} \neq 1$, has not been considered before, and numerical examples confirming the independent behavior predicted in regimes I and IV have also not been presented. Here we give clear numerical examples of all four types of behavior, and present a complete map of the different regimes, to be compared with the theoretical prediction given in Fig. 4.

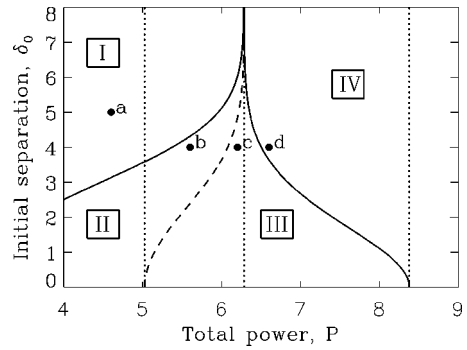

FIG. 4. Theoretically predicted regions of characteristic dynamics in the $P - \delta_0$ plane for $\eta_1 = \eta_2 = 4$, $\rho = 1$, $P_1 = P_2$, $\Delta = 2$, $\theta_{\mathrm{dif}} = 0.2$, and $\theta_{\mathrm{col}} = 1$. The solid curves represent δ_0^{dif} and δ_0^{col}, the dashed curve δ_0^{th}, and dotted lines indicate the limits $\mathcal{P}_0^{\mathrm{th}} = 5.03$, $\mathcal{P}_{\infty}^{\mathrm{th}} = 6.28$, and $\mathcal{P}_{\max} = 8.38$. Points $a - d$ indicate specific cases considered numerically in Figs. 5–8.

We now consider the particular symmetric case when $\eta_1 = \eta_2 = 4$, $\rho = 1$, $\Delta = 2$, and $P_1 = P_2 = P/2$. Then $\mathcal{P}_0^{\mathrm{th}} = 8\pi/5$, $\mathcal{P}_{\infty}^{\mathrm{th}} = 2\pi$, and the threshold and critical separations become

$$\begin{aligned}
\delta_0^{\mathrm{dif}} &= \sqrt{8 \ln\left(\frac{P/\theta_{\mathrm{dif}}}{8\pi - 4P}\right)}, \quad \mathcal{P}_{\min} < P < \mathcal{P}_{\infty}^{\mathrm{th}}, \\
\delta_0^{\mathrm{th}} &= \sqrt{8 \ln\left(\frac{P}{8\pi - 4P}\right)}, \quad \mathcal{P}_0^{\mathrm{th}} < P < \mathcal{P}_{\infty}^{\mathrm{th}}, \\
\delta_0^{\mathrm{col}} &= \sqrt{8 \ln\left(\frac{P/\theta_{\mathrm{col}}}{4P - 8\pi}\right)}, \quad \mathcal{P}_{\infty}^{\mathrm{th}} < P < \mathcal{P}_{\max},
\end{aligned} \tag{45}$$

where $\mathcal{P}_{\min} = 8\pi\theta_{\mathrm{dif}}/(4\theta_{\mathrm{dif}} + 1)$ and $\mathcal{P}_{\max} = 8\pi\theta_{\mathrm{col}}/(4\theta_{\mathrm{col}} - 1)$ for $\theta_{\mathrm{col}} > 0.25$, and $\mathcal{P}_{\max} = \infty$ for $\theta_{\mathrm{col}} \leqslant 0.25$. In Fig. 4 we show the theoretically predicted regimes in the $P - \delta_0$ plane for $\theta_{\mathrm{dif}} = 0.2$ and $\theta_{\mathrm{col}} = 1$.

To integrate Eqs. (2) and (3) numerically, we use a split step Fourier technique, with a resolution of $dx = dy = 0.1$, a step size of $dz = 10^{-2}$, and the initial condition (36) with $\Delta = 2$. Generally we have used 512×256 mesh points (512 in x), except for the examples shown in Figs. 5–8 and 10, where we have used 512×512 points. The allowable relative deviation of the conserved power from its initial value is 10^{-4}. In the theoretical discussion we assume that $\theta_{\mathrm{dif}} = 0.2$ and $\theta_{\mathrm{col}} = 1$, as in Fig. 4.

We identify the different scenarios by tracking the amplitude distribution $|E_n(x,0,z)|$ and the ''virtual point'' of maximum amplitude $[x_m(z), A(z)]$, which is found using a parabolic approximation for $|E_1(x,y,z)|$ between the three points x_0 and $x_0 \pm dx$, where (x_0, y_0) is the point of maximum $|E_1(x,y,z)|$ on the discrete mesh. Due to the special symmetry of the initial condition, the amplitude is the same for the two components, the separation the separation is $\delta(z) = 2x_m(z)$, and the virial is $I(z) = (2/P)\int r^2 |E_1|^2 \, d\vec{r}$, since $\langle \vec{r} \rangle = \vec{0}$.

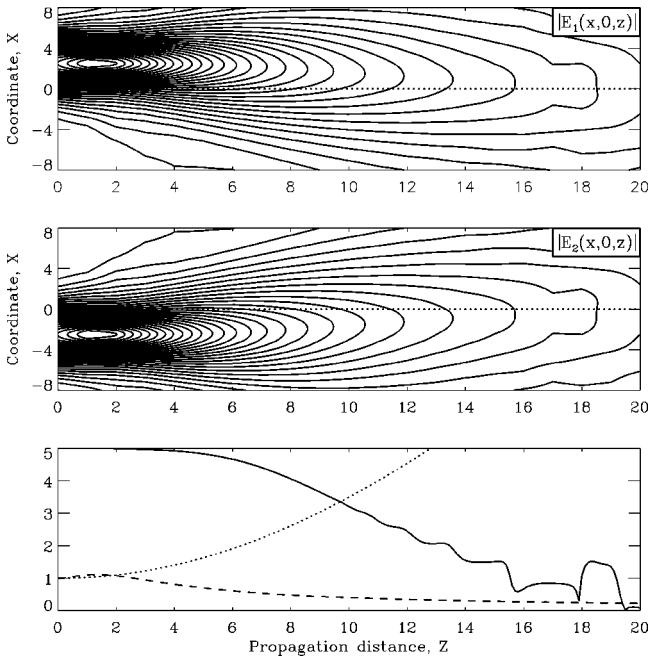

FIG. 5. Contour plot (30 equidistant levels between 0.01 and 0.458) of $|E_1(x,0,z)|$ (top) and $|E_2(x,0,z)|$ (middle), found by numerical integration of Eqs. (2) and (3) for $\eta_1=\eta_2=4$ and $\rho=1$. The bottom figure shows the corresponding evolution of the separation $|\delta(z)|$ (solid) and the normalized virial $I(z)/I(0)$ (dotted) and amplitude $A(z)/A(0)$ (dashed). The initial condition is Eq. (36) with $\Delta=2$, $P_1=P_2=2.3$, and $\delta_0=5$, corresponding to point *a* in Fig. 4.

In Fig. 5 we show an example from the low-power regime I with $P=4.6$ and $\delta_0=5$, above the critical separation $\delta_0^{\rm dif}=3.1$. Since the Hamiltonian is positive, $H=0.62$, and $|H_{\rm int}|=0.01$ is only 3% of $|H_{\rm free}|=0.31$, which is less than $\theta_{\rm dif}=20\%$, we expect both components to spread out while

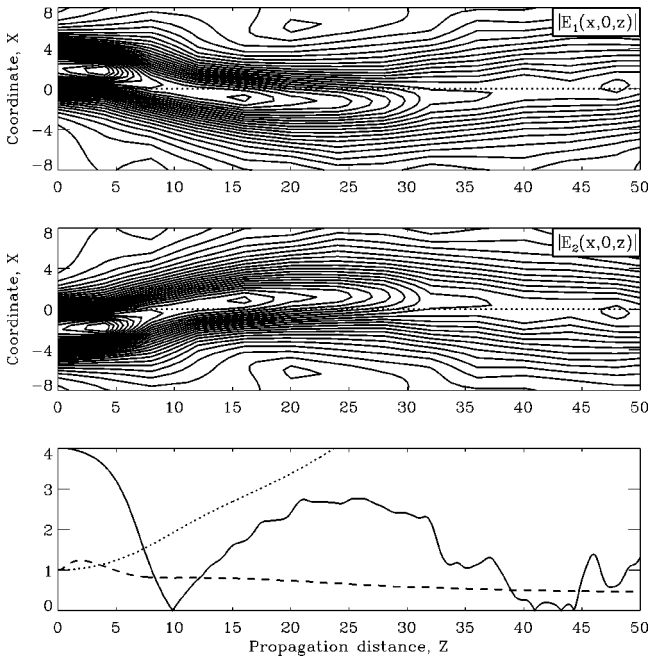

FIG. 6. As Fig. 5, but for $P_1=P_2=2.8$ and $\delta_0=4$, corresponding to point *b* in Fig. 4.

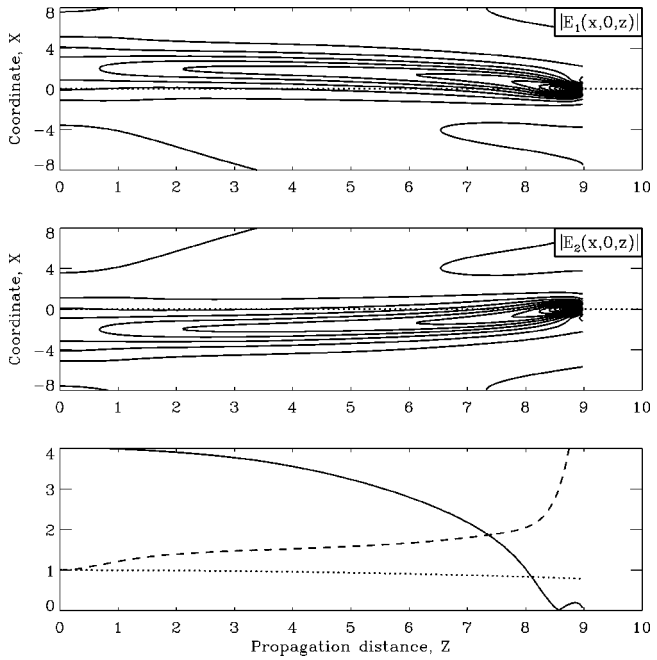

FIG. 7. As Fig. 5, but for $P_1=P_2=3.1$ and $\delta_0=4$, corresponding to point *c* in Fig. 4.

interacting only weakly. As expected, we see the spreading [$I(z)$ increases continuously], but despite the low power of the beams the interaction is still strong enough for them to attract and move towards each other. However, before they cross, the emitted radiation has propagated through the x boundaries and starts to influence the dynamics at around $z=12$, causing the until then monotonically decreasing separation to increase. At $z=19.5$ the radiation coming through the y boundaries even pushes the center y_0 away from $y_0=0$ (not shown).

We will define such a scenario, in which the spreading and consequent decay of the amplitude is so fast that $A(z)$

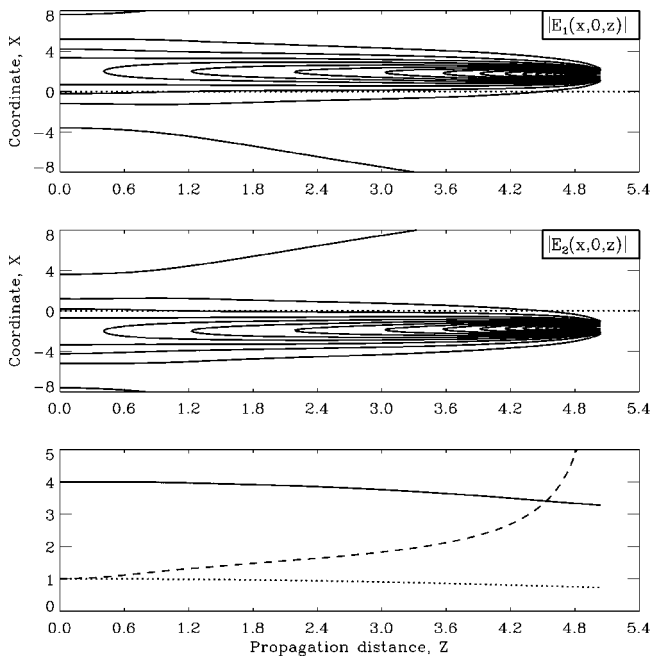

FIG. 8. As Fig. 5, but for $P_1=P_2=3.3$ and $\delta_0=4$, corresponding to point *d* in Fig. 4.

drops to half its initial value $A(0)$ before the beams have crossed as *independent spreading*. The attraction still observable in this regime can be explained from geometrical optics, in that the opposite beam acts as a gradient in the refractive index.

In Fig. 6 we show an example from the low-power regime II with $P=5.6$ and $\delta_0=4$, in between the critical separation $\delta_0^{\rm dif}=4.3$ and the threshold separation $\delta_0^{\rm th}=2.4$. In this case the Hamiltonian is still positive, $H=0.11$, but now $|H_{\rm int}|=0.04$ is 27% of $|H_{\rm free}|=0.15$, which is more than $\theta_{\rm dif}=20\%$. Thus we expect the interaction to be strong, even though the beams will ultimately spread out. As expected, we see that the beams attract each other strongly and cross at $z=9.83$, and even a second time at around $z=41$, although influenced by radiation coming through the boundaries at this point.

It appears as if they perform damped oscillations about the center of mass $(x,y)=(0,0)$ that could possibly continue over an even longer distance if the initial separation had been closer to the threshold separation for collapse. Oscillations in the separation between the beams in the diffraction regime, but close to the threshold $\delta_0^{\rm th}(P)$, were predicted analytically in [16] from variational calculations. However, the oscillations were found to increase in amplitude. This is clearly an artifact of the variational approach and its main approximation, in which the solution is assumed to keep a prescribed test profile during evolution.

We define such a scenario, in which the beams cross at least once before the amplitude has decayed to half its initial value $A(0)$, as *fusion+spreading*.

In Fig. 7 we show an example from the low-power region of regime III with $P=6.2$ and $\delta_0=4$, below the threshold separation $\delta_0^{\rm th}=4.8$. In this case the Hamiltonian is slightly negative, $H=-0.03$, and $|H_{\rm int}|=0.05$ is dominant compared to $|H_{\rm free}|=0.02$. Thus we expect the components to interact strongly and cross at least once before eventually collapsing. This is also confirmed by the numerical simulation, which shows that the beams cross at $z=8.57$, with the amplitude blowing up soon thereafter at $z=8.98$, as they again come close together after one cycle of a highly damped oscillation, with $\delta(z)$ reaching only $\delta(z)=-0.19$.

We define such a scenario, in which the beams cross at least once before collapsing, as *fusion+collapse*.

Note that the amplitude blows up before all the power has collapsed into the single point $(x,y)=(0,0)$ and the virial has reached zero, which is a well-known phenomenon in collapse studies (see the discussion in Sec. III). In general, the collapse distance predicted from virial theory should be viewed only as an upper limit of the actual collapse distance.

In Fig. 8 we show an example from the high-power regime IV with $P=6.6$ and $\delta_0=4$, slightly above the critical separation $\delta_0^{\rm col}=3.6$. In this case the Hamiltonian is negative, $H=-0.14$, with $|H_{\rm int}|=0.06$ being 75% of $|H_{\rm free}|=0.08$, i.e., below $\theta_{\rm col}=1$. Thus we expect that the components will attract each other, but not be able to fuse before collapsing almost at their initial position. This is confirmed by the numerical simulation, showing that the beams collapse at $z=5.04$, with the separation having only decreased by 18% to $\delta(z)=3.28$.

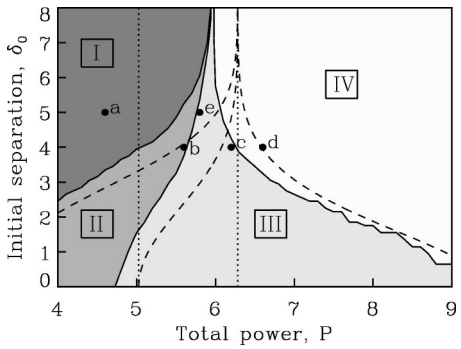

FIG. 9. Numerically found regions of characteristic dynamics in the $P-\delta_0$ plane for $\eta_1=\eta_2=4$, $\rho=1$, $P_1=P_2$, $\Delta=2$. Dashed curves represent $\delta_0^{\rm dif}$, $\delta_0^{\rm th}$, and $\delta_0^{\rm col}$ for $\theta_{\rm dif}=0.25$ and $\theta_{\rm col}=0.75$. Dotted lines indicate $\mathcal{P}_0^{\rm th}=5.03$ and $\mathcal{P}_\infty^{\rm th}=6.28$.

We define such a scenario, in which the beams do not cross before collapsing, as *independent collapse*.

Using these definitions of the different types of characteristic dynamics, we have made extensive numerical calculations and recorded the regions in which they occur. The results are shown in Fig. 9, which confirms the existence of four regions of different dynamical behavior.

We see that the numerically found power threshold for collapse is slightly lower, but otherwise follows the theoretical curve $P^{\rm th}(\delta_0)$. The shift of $\Delta P\approx 0.3$ can be attributed to three effects. First of all, the Gaussian initial condition differs from the stationary ground-state solutions found in Sec. IV, and thus power is lost to radiation in the initial ''adjustment'' phase (see Figs. 5, 6, and 10). Thus $\Delta P\approx 0.3$ corresponds approximately to the difference between $\mathcal{P}_\infty^{\rm th}=2\pi=6.28$ calculated from the Gaussian initial condition, and $\mathcal{P}_\infty^{\rm th}=P_{\rm NLS}/2=5.85$, which is the exact threshold in the limit $\delta_0\to\infty$, where the dynamical equations reduce to two uncoupled 2D NLS equations. Furthermore, a certain amount of power is lost to radiation during collision, and therefore does not participate in the collapse process. Finally, it is well known that the discreteness imposed by the numerical grid lowers the threshold power [26].

Taking into account the shift $\Delta P\approx 0.3$ towards lower powers, the limit between independent and strongly coupled (fusion) behavior in the low-power diffraction region is optimally reproduced by the estimated critical separation $\delta_0^{\rm dif}(P)$ when $\theta_{\rm dif}=0.25$. From the high-power collapse region we see that $\theta_{\rm col}=1$ is not necessary. Instead we find that $\theta_{\rm col}=0.75$ optimizes the fit of the estimated critical separation $\delta_0^{\rm col}(P)$ to the numerical data.

The damped oscillation in the separation between two incoherently coupled beams, which was observed in Fig. 6, is of particular interest. Since such oscillations require that the beams keep their shape over a considerable distance, they can only be observed for beam powers close to the threshold for collapse $\mathcal{P}^{\rm th}(\delta_0)$ (as also found in [16]) where the beams are marginally stable with the collapse length (or diffraction length) going to infinity. In Fig. 10 we show an example of damped oscillations in the low-power collapse regime III, where the beams eventually collapse after having crossed four times. Such damped oscillations ending with fusion and collapse as a single entity were recently predicted from variational calculations [16]. In contrast to the diffraction

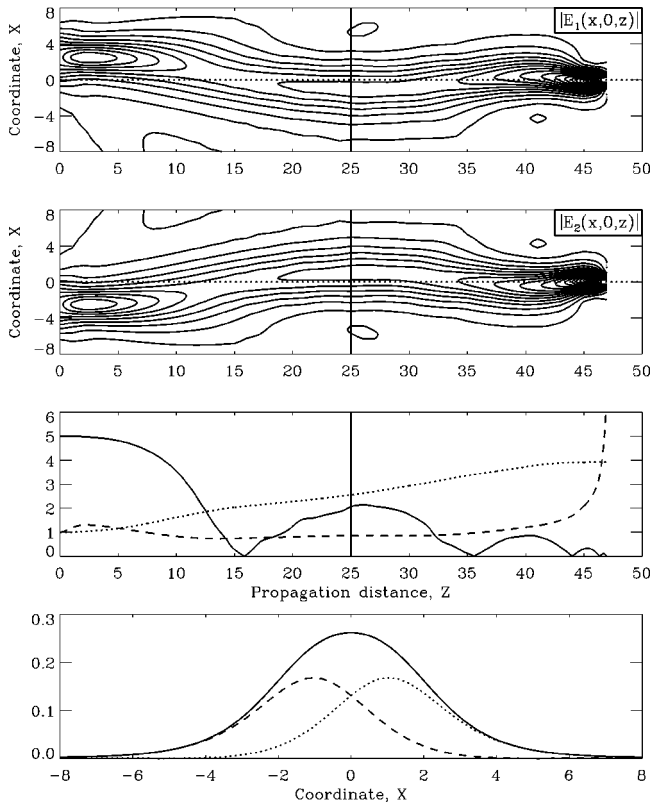

FIG. 10. As Fig. 5, but for $P_1=P_2=2.9$ and $\delta_0=5$, corresponding to point *e* in Fig. 9. The additional bottom figure shows the total intensity profile $|E_1(x,0,z)|^2+|E_2(x,0,z)|^2$ (solid) and the individual profiles $|E_n(x,0,z)|^2$ (dashed and dotted) at $z=25$, marked by a vertical line in the upper three figures.

regime, where the variational approach predicted that the amplitude increased, its main assumption of a constant test profile seems therefore to be a good approximation in the collapse regime (see the discussion in connection with Fig. 6).

We note that no such oscillations have been observed for two coherently coupled Gaussian beams described by the single-component 2D NLS equation [15], which is similar to Eqs. (2) and (3) in the sense that it also allows no stable solitary waves towards which the beams can evolve. The reason for this is that one can only compare the evolution of the total intensity in the two systems. This is confirmed by the profiles of the total intensity shown in Fig. 10, from which we see that the two beams cannot be separated, but appear as a single hump even when they are farthest away after the first crossing. The reason why we can separate them is that they are incoherent, i.e., they each have a distinct mark, such as, e.g., orthogonal polarizations or different frequencies. In the NLS equation, when two coherent beams (two humps in the amplitude of the NLS solution) are too close, they have no such individual mark, and therefore they cannot be separated, but appear as a single hump solution.

In isotropic bulk media that allow the existence of stable 2D solitary waves, such as saturable Kerr media, fusion of two input beams into a single soliton or two solitons forming a bound state can be observed [28].

To illustrate the specific transitions between the different regimes, we show in Fig. 11 the diffraction distance Z_{diff} at which the amplitude has decayed to half its initial value, the

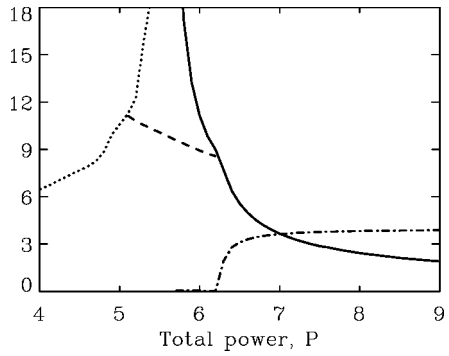

FIG. 11. Z_{coll} (solid), Z_{diff} (dotted), Z_{cross} (dashed), and Δ_{sep} (dash-dotted) versus P for $\delta_0=4$, corresponding to horizontal cuts in Fig. 9.

distance of the first crossing Z_{cross}, the collapse distance Z_{coll}, and the distance between the center of the two components at collapse $\Delta_{\mathrm{sep}}=|\delta_0(Z_{\mathrm{coll}})|$, versus the total power P for fixed initial separation $\delta_0=4$.

At high powers we see that the collapse distance is short, the crossing distance is undefined, and $\Delta_{\mathrm{sep}}\approx\delta_0$, i.e., the beams collapse individually and we are in regime IV. Upon decreasing the power, the collapse distance increases and the separation Δ_{sep} decreases. When Δ_{sep} reaches zero at $P=6.2$ the crossing distance becomes well-defined and bifurcates from the Z_{coll} curve, i.e., we have (at least one) crossing and subsequent collapse and we enter into regime III. Upon decreasing the power further, the collapse distance goes to infinity and is no longer defined below the threshold $P=5.6$, where we instead have (at least one) crossing with subsequent diffraction and we enter into regime II. Finally, below $P=4.7$, the beams are no longer able to cross before the amplitude has decayed to half its initial value ($Z_{\mathrm{diff}}<Z_{\mathrm{cross}}$). Thus Z_{cross} is no longer defined and we enter into regime I.

In Fig. 12 we fix instead the power and show the dependence on the separation δ_0. For low powers $P=5.6$ we see that both the crossing and collapse distances are well-defined, with $Z_{\mathrm{cross}}<Z_{\mathrm{coll}}$ and $\Delta_{\mathrm{sep}}=0$. Thus we have (at least one) crossing with subsequent collapse in regime III. Increasing δ_0, the crossing and collapse distances also increase. When the beams are further separated than $\delta_0=3.8$, they no longer collapse, and we enter into regime II of fusion and diffraction. Eventually the beams are so far apart ini-

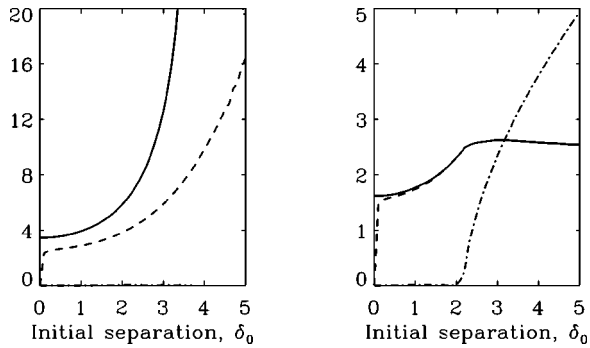

FIG. 12. Z_{coll} (solid), Z_{cross} (dashed), and Δ_{sep} (dash-dotted) versus δ_0 for $P=5.6$ (left) and $P=7.8$ (right), corresponding to vertical cuts in Fig. 9.

tially ($\delta_0 > 6.0$) that they diffract independently, and we are in regime I.

For high powers $P = 7.8$ there is always collapse. At $\delta_0 = 1.9$ there is a transition between regimes III and IV of coupled and uncoupled collapse. Starting at small initial separations the Z_{cross} and Z_{coll} curves bifurcate into each other at this value, and the collapse separation starts to increase. For sufficiently large separations both components collapse at the point of initial excitation, $\Delta_{\text{sep}} = \delta_0$, and the collapse distance saturates to the constant value $Z_{\text{coll}} = 2.5$.

VI. SUMMARY AND DISCUSSION

We have studied the properties of two incoherently coupled localized waves in bulk cubic media with two transverse dimensions, described by the equations

$$i\partial_z E_1 + (\partial_x^2 + \partial_y^2)E_1 + (\eta_1 |E_1|^2 + \rho |E_2|^2)E_1 = 0,$$

$$i\partial_z E_2 + (\partial_x^2 + \partial_y^2)E_2 + (\eta_2 |E_2|^2 + \rho |E_1|^2)E_2 = 0,$$

where $\rho = \pm 1$. This represents the simplest scaled version of a general physical system that has equal diffraction coefficients, but can include walk-off. The main scope of the paper has been to give a complete description of the possible dynamics, both analytically and numerically.

As a first step we have used virial theory to derive a sufficient condition for collapse (negative Hamiltonian, $H < 0$), which is valid for arbitrary values of the parameters, and a sufficient condition for spreading (low power of both components, $P_n < P_n^{\text{th}}$), which is valid for $\rho \geqslant 0$ and $\eta_n \geqslant -\rho$. These conditions were derived in [10] and [14], respectively, so we have only given a brief summary for the present notation.

However, in doing so we have emphasized an interesting property of this multicomponent system: The system conserves the individual power in each component, but, nevertheless, when only one of the components has a power below the threshold P_n^{th}, both components can still collapse, even when the Hamiltonian is positive, and the beam is given a strong prefocusing at the input (negative initial derivative of the virial). Furthermore, the use of the Schwarz inequality in the derivation means that P_n^{th} can significantly underestimate the actual threshold power for collapse when the two components are initially separated. These facts underline that $H < 0$ and $P_n < P_n^{\text{th}}$ are *sufficient* conditions.

To see whether the system has stable bound states towards which a given input condition can evolve, we have numerically found the different types of families of stationary bright solitonlike solutions, which exist for positive SPM coefficients, $\eta_n > 0$. Sech-profile solutions calculated using variational techniques are found to accurately represent the numerically found solutions. Simple calculations show that the Hamiltonian is zero on the soliton solutions, and that the derivative of the power with respect to the soliton eigenvalue is also zero.

This predicts that the soliton solutions are so-called marginally stable, just as for the 2D NLS equation. In other words, this theoretical result suggests that the solitons are unstable, which is confirmed numerically for a number of test cases, where the solutions were observed to collapse after a finite propagation distance. A rigorous proof of this instability would be an important subject for further studies.

In our numerical studies we have considered Gaussian initial conditions, for which the Hamiltonian can be calculated explicitly, and the sufficient conditions for collapse and spreading reduce to the total power being above and below certain threshold values, $P > \mathcal{P}_{\text{up}}^{\text{th}}(\delta_0)$ and $P < \mathcal{P}_{\text{low}}^{\text{th}}$, respectively, where the threshold for collapse depends on the initial separation δ_0 of the two components.

Fixing $\rho = 1$ and tracing the collapse threshold in the (η_1, η_2) space, we have numerically confirmed these sufficient conditions for the particular case when the two components are identical, $E_1(\vec{r},0) = E_2(\vec{r},0)$, and superimposed, $\delta_0 = 0$. In doing so we have emphasized an important difference between symmetric systems with $\eta_1 = \eta_2$ and $E_1(\vec{r},0) = E_2(\vec{r},0)$, and asymmetric systems with $\eta_1 \neq \eta_2$ and/or $E_1(\vec{r},0) \neq E_2(\vec{r},0)$: The sufficient conditions for collapse and spreading are to a good approximation necessary conditions also, *only* if the system is symmetric. This has not been considered in the literature so far, and is important when one wants to accurately predict the regions of different dynamical behavior.

Finally we have studied the more general case when the two components are initially separated. In view of the above mentioned result we have for simplicity considered only nearly symmetric systems in the theoretical treatment. In this case $H = 0$, or equivalently $P = \mathcal{P}_{\text{up}}^{\text{th}}(\delta_0)$, gives an accurate prediction of the actual threshold for collapse.

Using virial theory and the internal structure of the Hamiltonian, we have found the regions of different dynamical behavior in terms of the total power and the initial separation. The condition $H(\delta_0) = H_{\text{free}} + H_{\text{int}}(\delta_0) = 0$ separates the phase space into two regions with collapse and spreading, respectively. From the relative strength of the interaction part $|H_{\text{int}}(\delta_0)|$ and the free part $|H_{\text{free}}|$, each of these regions is then separated into two subregions of uncoupled and coupled behavior. To do so we have had to introduce two additional parameters θ_{dif} and θ_{col}, which gives the fraction $|H_{\text{int}}(\delta_0)/H_{\text{free}}|$, or the degree of initial overlap, required for the attraction to be strong enough to cause the components to cross before a collapse occurs (θ_{col}), or before they have diffracted so much that they are essentially in the linear regime (θ_{dif}). We have presented heuristical arguments for the approximate values of θ_{dif} and θ_{col}, but in principle they must be determined numerically.

In summary, the theory gives three characteristic power-dependent initial separations, which divides the phase space into four regions of different dynamical behavior. For the symmetric case with $\rho = 1, \eta_n = 4$, and identical initial conditions for the two components, we have performed extensive numerical calculations and traced the characteristic separations. The results verify the predictions of the four regions and give the fractions $\theta_{\text{col}} \approx 0.75$ and $\theta_{\text{dif}} \approx 0.25$. Thus, as heuristical arguments predict, the initial overlap must be larger in the collapse region than in the diffraction region in order for the components to fuse. A numerical example of the dynamics in each region is presented.

This completes the pioneering work of McKinstrie and Russel [10], who first used virial theory to find the charac-

teristic separation dividing collapsing and diffracting solutions, and gave two numerical examples of fusion with subsequent collapse and spreading. Furthermore, it completes the recent work of Bergé [16], who first used the internal structure of the Hamiltonian to separate the collapse region into subregions of fusion before collapse and independent collapse. Here the fractions θ_{dif} and θ_{col} were not introduced, but $|H_{\mathrm{int}}(\delta_0)| = |H_{\mathrm{free}}|$ was assumed to give the separatrix, which is why the specific separation of the diffraction region into coupled and uncoupled behavior was not determined.

Close to the threshold for collapse the solution is marginally stable and the two components keep their shape over a considerable distance, with the collapse or diffraction length going to infinity. In this region we have observed that the components were able to cross several times before fusing. We have shown two numerical examples of this oscillatory behavior, in which the two components performed damped oscillations around the center of mass, before eventually collapsing and diffracting as one entity, respectively.

Such oscillations of initially close Gaussian beams with medium powers were predicted from variational calculations [16]. In the collapse regime the oscillations were found to be damped, corresponding to what we observe. However, in the diffraction regime the amplitude of the oscillations were found to increase indefinitely, which contradicts our numerical results. This is clearly an artifact of the variational approach and its main approximation, in which the solution is assumed to keep a prescribed test profile during evolution. An interesting subject for further studies would be to adjust the variational approach appropriately, such as to be able to theoretically predict the damped oscillations in the diffraction regime also.

Here and in [10,16] specific examples have been given for a symmetric system. We do not expect the existence of the four different regions to change qualitatively for asymmetric systems, but in any case, a thorough study of the asymmetric case would be important. Furthermore, the influence of the four-wave-mixing terms, which are neglected in our model, should be investigated.

ACKNOWLEDGMENTS

We acknowledge useful discussion with D.E. Edmunson, W.Z. Krolikowski, and M.R. Schmidt. This work was supported by the Australian Department of Industry, Science and Tourism, the Danish Natural Science Research Council (SNF) under Grant No. 9600852, and the INTAS Grant No. 96-0413.

[1] G.P. Agrawal, *Nonlinear Fiber Optics* (Academic Press, San Diego, 1989).
[2] A.C. Newell and J.V. Moloney, *Nonlinear Optics* (Addison-Wesley, Redwood City, 1992).
[3] V.E. Zakharov and A.B. Shabat, Zh. Eksp. Teor. Fiz. **61**, 118 (1971) [Sov. Phys. JETP **34**, 62 (1972)].
[4] J.J. Rasmussen and K. Rypdal, Phys. Scr. **33**, 481 (1986).
[5] D.N. Christodoulides, T.H. Coskun, M. Mitchell, and M. Segev, Phys. Rev. Lett. **78**, 646 (1997).
[6] M. Mitchell, Z. Chen, M.F. Shih, and M. Segev, Phys. Rev. Lett. **77**, 490 (1996).
[7] M. Mitchell and M. Segev, Nature (London) **387**, 880 (1997).
[8] A.L. Berkhoer and V.E. Zakharov, Zh. Éksp. Teor. Fiz. **58**, 903 (1970) [Sov. Phys. JETP **31**, 486 (1970)].
[9] O. Bang, J. Opt. Soc. Am. B **14**, 51 (1997).
[10] C.J. McKinstrie and D.A. Russell, Phys. Rev. Lett. **61**, 2929 (1988).
[11] S.V. Manakov, Zh. Éksp. Teor. Fiz. **65**, 505 (1973) [Sov. Phys. JETP **38**, 248 (1974)].
[12] J.U. Kang, G.I. Stegeman, J.S. Aitchison, and N. Akhmediev, Phys. Rev. Lett. **76**, 3699 (1996).
[13] N.N. Akhmediev and A. Ankiewicz, *Solitons: Nonlinear Pulses and Beams* (Chapman & Hall, London, 1997).
[14] L. Bergé, O. Bang, J.J. Rasmussen, and V.K. Mezentsev, Phys. Rev. E **55**, 3555 (1997).
[15] L. Bergé, M.R. Schmidt, J. Juul Rasmussen, P.L. Christiansen, and K.Ø. Rasmussen, J. Opt. Soc. Am. B **14**, 2550 (1997).
[16] L. Bergé, Phys. Rev. E **58** 6606 (1998).
[17] M. Ohta, Nonlinear Anal. Theor. Methods Appl. **26**, 933 (1996).
[18] M. Grillakis *et al.*, J. Funct. Anal. **74**, 160 (1987); **94**, 308 (1990).
[19] M.G. Vakhitov and A.A. Kolokolov, Radiophys. Quantum Electron. **16**, 783 (1975).
[20] M.I. Weinstein, Commun. Math. Phys. **87**, 567 (1983).
[21] K. Rypdal, J.J. Rasmussen, and K. Thomsen, Physica D **16**, 339 (1985).
[22] L. Bergé, Phys. Rep. **303**, 259 (1998).
[23] O. Bang, Yu.S. Kivshar, A.V. Buryak, A. De Rossi, and S. Trillo, Phys. Rev. E **58**, 5057 (1998).
[24] A.V. Buryak, Y.S. Kivshar, and S. Trillo, Opt. Lett. **20**, 1961 (1995).
[25] D. Anderson, M. Bonnedal, and M. Lisak, Phys. Fluids **22**, 1838 (1979).
[26] O. Bang, J.J. Rasmussen, and P.L. Christiansen, Nonlinearity **7**, 205 (1994).
[27] O. Bang, L. Bergé, and J.J. Rasmussen, Opt. Commun. **146**, 231 (1998).
[28] S. Gatz and J. Herrmann, J. Opt. Soc. Am. B **14**, 1795 (1997).